

# Targeting Tuberculosis and Malaria through Inhibition of Enoyl Reductase

COMPOUND ACTIVITY AND STRUCTURAL DATA\*

Received for publication, November 25, 2002, and in revised form, February 14, 2003  
Published, JBC Papers in Press, February 26, 2003, DOI 10.1074/jbc.M211968200

Mack R. Kuo‡, Hector R. Morbidoni§¶, David Alland||, Scott F. Sneddon\*\*, Brian B. Gourlie\*\*, Mark M. Staveski\*\*, Marina Leonard\*\*, Jill S. Gregory\*\*, Andrew D. Janjigian\*\*, Christopher Yee\*\*, James M. Musser‡‡, Barry Kreiswirth§§, Hiroyuki Iwamoto‡, Remo Perozzo‡, William R. Jacobs, Jr.§¶¶, James C. Sacchettini‡|||, and David A. Fidock§

From the ‡Department of Biochemistry and Biophysics, Texas A & M University, College Station, Texas 77843, the §Department of Microbiology and Immunology and ¶¶Howard Hughes Medical Institute, Albert Einstein College of Medicine, Bronx, New York 10461, ||Division of Infectious Diseases and the Center for Emerging Pathogens, New Jersey Medical School, Newark, New Jersey 07103, \*\*Genzyme Drug Discovery, Genzyme Corp., Cambridge, Massachusetts 02139-1562, ‡‡Laboratory of Human Bacterial Pathogenesis, Division of Intramural Research, NIAID, National Institutes of Health, Rocky Mountain Laboratories, Hamilton, Montana 59840, and §§Public Health Research Institute TB Center, New York, New York 10016

Tuberculosis and malaria together result in an estimated 5 million deaths annually. The spread of multi-drug resistance in the most pathogenic causative agents, *Mycobacterium tuberculosis* and *Plasmodium falciparum*, underscores the need to identify active compounds with novel inhibitory properties. Although genetically unrelated, both organisms use a type II fatty-acid synthase system. Enoyl acyl carrier protein reductase (ENR), a key type II enzyme, has been repeatedly validated as an effective antimicrobial target. Using high throughput inhibitor screens with a combinatorial library, we have identified two novel classes of compounds with activity against the *M. tuberculosis* and *P. falciparum* enzyme (referred to as InhA and PfENR, respectively). The crystal structure of InhA complexed with NAD<sup>+</sup> and one of the inhibitors was determined to elucidate the mode of binding. Structural analysis of InhA with the broad spectrum antimicrobial triclosan revealed a unique stoichiometry where the enzyme contained either a single triclosan molecule, in a configuration typical of other bacterial ENR:triclosan structures, or harbored two triclosan molecules bound to the active site. Significantly, these compounds do not require activation and are effective against wild-type and drug-resistant strains of *M. tuberculosis* and *P. falciparum*. Moreover, they provide broader chemical diversity and elucidate key elements of inhibitor binding to InhA for subsequent chemical optimization.

Despite the worldwide ravages of tuberculosis and malaria, chemotherapeutic regimens against these two diseases have remained largely unchanged. For over 40 years, isoniazid (isonicotinic acid hydrazide (INH)<sup>1</sup>) has been utilized as a frontline agent in drug mixtures to treat *Mycobacterium tuberculosis*, whereas *Plasmodium falciparum* malaria has primarily been treated with chloroquine or pyrimethamine-sulfadoxine. The emergence of strains resistant to these and all other widely available and affordable antitubercular and antimalarial drugs, due in part to the limited number of pathways being targeted, makes it essential to identify lead compounds active against novel targets.

Of particular interest from a drug discovery perspective, *M. tuberculosis* and *P. falciparum* share enzymatic components of the type II fatty acid biosynthetic pathway (FAS-II) (1, 2). In the case of *Mycobacterium*, FAS-II co-exists with the type I (FAS-I) pathway, a situation that is unique to this genus. Here FAS-I is responsible for *de novo* synthesis of the C16–C26 fatty acids, used for production of phospholipids and as primers for complex lipids. The FAS-II system extends these fatty acids up to C56 to make the long chain precursors required for the synthesis of cell wall-associated mycolic acids that are specific to Mycobacteria. For *Plasmodium*, FAS-II is the only fatty acid pathway whose enzymatic components reside in the apicoplast, a unique plastid organelle that is essential to the development of the parasite (3). The apicoplast is thought to have derived from a cyanobacterial endosymbiont (4–6), whose function in plasmodial parasites is still undetermined but appears to include fatty acid and isoprenoid biosynthesis (2, 7). The discovery of FAS-II in the malaria parasite was surprising as this pathway had been found previously only in plants, prokaryotes, and Archaea, where it is responsible for the synthesis of fatty acids up to C16 and C18 that are required for membrane biogenesis. No FAS-I homologs can be found in the gene sequence of *P. falciparum* or, for that matter, in any of the related Apicomplexan parasites. Whereas FAS-II consists of several

\* This work was supported in part by National Institutes of Health Grant AI43268 and the Robert A. Welch Foundation (to J. C. S.) and by a Burroughs Wellcome Fund New Initiatives in Malaria Research Award (to D. A. F. and W. R. J.). The costs of publication of this article were defrayed in part by the payment of page charges. This article must therefore be hereby marked "advertisement" in accordance with 18 U.S.C. Section 1734 solely to indicate this fact.

The atomic coordinates and structure factors (code 1P44 and 1P45) have been deposited in the Protein Data Bank, Research Collaboratory for Structural Bioinformatics, Rutgers University, New Brunswick, NJ (<http://www.rcsb.org/>).

¶ Career Investigator of the Consejo de Investigaciones de la Universidad Nacional de Rosario, Argentina.

||| To whom correspondence should be addressed: Dept. of Biochemistry and Biophysics, Texas A & M University, Biochemistry and Biophysics Bldg., Rm. 221, College Station, TX 77843. E-mail: sacchett@tamu.edu.

<sup>1</sup> The abbreviations used are: INH, isonicotinic acid hydrazide; ACP, acyl carrier protein; Me<sub>2</sub>SO, dimethyl sulfoxide; ENR, enoyl reductase; FAS-I, fatty-acid synthase type I; FAS-II, fatty-acid synthase type II; InhA, the translation product of the *inhA* gene; MIC, minimum inhibitory concentration; PfENR, the translation product of the *pfenr* gene; PIPES, 1,4-piperazinediethanesulfonic acid.

distinct enzymes, all the enzyme activities required for FAS-I fatty acid elongation reside on a single, large multifunctional enzyme.

Several observations demonstrate that the FAS-II enzymes are ideal candidates for drug discovery. First, fatty acid biosynthesis has been validated repeatedly as an effective antimicrobial target. For instance, FAS-II enzymes have been identified as the targets of several widely used antibacterials including INH, diazaborines (8), triclosan (9), and thiolactomycin (10–13). Second, FAS-II is absent in humans, superceded by a FAS-I system that is insensitive to many FAS-II inhibitors. Moreover, the cell wall/membrane component fatty acyl chains appear to be essential to microbe division and metabolism, and microbial pathogens are apparently unable to survive simply by scavenging host fatty acids. The enzyme target of most of the known FAS-II antimicrobial compounds is ENR, which catalyzes the final enzymatic step in the elongation cycle of the FAS-II pathway, converting *trans*-2-enoyl-ACP to acyl-ACP in a NADH-dependent reaction. The *M. tuberculosis* ENR, commonly known as InhA or FabI, has been shown to be the target of the first line anti-tubercular INH (14). This enzymatic inhibition has been shown in the fast-growing model organism *Mycobacterium smegmatis* to inhibit mycolic acid synthesis and induce cell lysis (15). The activity of INH is dependent on its activation to an acyl radical by a manganese-dependent reaction catalyzed by the catalase/peroxidase enzyme, KatG (16). The INH acyl-radical forms a covalent adduct with NADH, producing binding interactions with InhA. Mutations in KatG have been linked to clinical resistance in ~50% of the newly diagnosed cases of INH-resistant tuberculosis (17). Compounds that do not require activation and that directly target ENR would circumvent this resistance mechanism. Unlike INH, the diazaborines and triclosan do not require activation, although their utility for human treatment is limited due to their respective toxicity (18) and poor solubility (19).

Triclosan has been reported recently (19–21) to inhibit *P. falciparum* ENR (PfENR), confirming the FAS-II pathway as a promising antimalarial chemotherapeutic target. Inhibition with thiolactomycin, a fairly nonspecific inhibitor of the FAS-II condensing enzyme, was also reported, albeit at high (~50  $\mu\text{M}$ ) concentrations (2). In an extension of this research, the crystal structure of PfENR complexed with triclosan was recently solved, indicating a high degree of structural conservation between this malarial enzyme and microbial and plant ENRs (21). *In vitro* whole-cell studies indicated killing of multidrug-resistant and drug-sensitive *P. falciparum* strains with low micromolar concentrations of triclosan and recently with triclosan analogs (19–21).

To extend the range of pharmacophores from which to develop more potent and pharmacologically suitable ENR inhibitors, we have undertaken a high-throughput screen against the *M. tuberculosis* enzyme, InhA. Here we report the identification and preliminary evaluation of two novel inhibitors derived from this screen, Genz-8575 and Genz-10850, which demonstrate activity against drug-sensitive and drug-resistant strains of both *M. tuberculosis* and *P. falciparum*. We also present structural data on the binding of one of these compounds, and triclosan, to purified InhA and PfENR. These structural data provide insights into the structure-activity relationships of these compounds and serve for further chemical refinement of inhibitors of this established antimicrobial target.

#### EXPERIMENTAL PROCEDURES

**Analysis of [ $^{14}\text{C}$ ]NAD $^{+}$  Binding to InhA**—Gel filtration chromatography was utilized to separate InhA-bound [ $^{14}\text{C}$ ]NAD $^{+}$  from free [ $^{14}\text{C}$ ]NAD $^{+}$  (22). For this, a 1  $\times$  12-cm Sephadex G-25 column was

equilibrated in 0.1 M PIPES, pH 6.8, at 25  $^{\circ}\text{C}$ . Samples (100  $\mu\text{l}$ ) containing combinations of InhA, [ $^{14}\text{C}$ ]NAD $^{+}$ , and triclosan were then applied. The column was eluted with the same buffer, and fractions were collected. Fractions were counted in ScintiVerse scintillation solution.

**Crystallization and Data Collection**—Recombinant InhA was produced, purified, and crystallized using methods described previously (23). Hanging drop methods were utilized to co-crystallize InhA-inhibitor complexes. For the InhA-Genz-10850 complex, the product analog was solubilized in 100% Me $_2$ SO and added dropwise at room temperature to a dilute InhA solution containing NADH. The final molar ratios of the mixture were 1 InhA active site to 100 NADH to 1.5 Genz-10850, in 1% (v/v) Me $_2$ SO. The mixture was concentrated to 10 mg/ml, and the crystals were produced in wells containing 12% polyethylene glycol 3350, 150 mM ammonium acetate, and 100 mM [(carbamoylmethyl)imino]diacetic acid, pH 6.8, using the vapor diffusion method. The crystals were of the space group C2 with unit cell dimensions  $a = 101.01 \text{ \AA}$ ,  $b = 83.31 \text{ \AA}$ ,  $c = 193.07 \text{ \AA}$  ( $\alpha = 90^{\circ}$ ,  $\beta = 95.21^{\circ}$ ,  $\gamma = 90^{\circ}$ ) and contained 6 molecules per asymmetric unit. X-ray diffraction data of the InhA:Genz-10850 crystal was collected using a MacScience DIP2030 image plate detector coupled to a Rigaku x-ray generator utilizing a copper rotating anode (CuK $_{\alpha}$ ,  $\lambda = 1.54 \text{ \AA}$ ). The detector was placed 200 mm from the crystal with no offset in the  $2\theta$  angle. Each data frame was exposed for 10 min and consisted of a 1.5 $^{\circ}$  rotation of the crystal. For the InhA-triclosan complex, crystals bound to triclosan were formed in the I2 $_1$ 2 $_1$ 2 $_1$  space group, unit cell  $a = 94.8 \text{ \AA}$ ,  $b = 103.9 \text{ \AA}$ ,  $c = 189.6 \text{ \AA}$ ,  $\alpha = \beta = \gamma = 90^{\circ}$ , via hanging drop vapor diffusion experiments, with 100 mM Tris, pH 8.0, in the well solution. InhA was concentrated to 5 mg/ml and crystallized upon the introduction of triclosan to a solution with a 1:2:1 stoichiometric ratio of InhA, NAD $^{+}$ , and triclosan. Increasing the concentration of triclosan to yield a 1:2:2 (or higher) stoichiometric ratio resulted in microcrystals that did not diffract. Data were collected to 2.6  $\text{ \AA}$  resolution at 120 K. X-ray diffraction data of the InhA:triclosan crystal were collected at the Advanced Photon Source (Beamline 14-BM-C) at a wavelength of 1.0  $\text{ \AA}$ . The detector was placed 200 mm from the crystal. Each data frame was exposed for 30 s and consisted of a 1.0 $^{\circ}$  rotation of the crystal. All images were autoindexed, integrated, and scaled together using the DENZO and SCALEPACK software packages (24).

**Structure Determination and Refinement**—Initial phases were obtained using molecular replacement, with a single subunit of InhA derived from the hexagonal crystal form of InhA (Protein Data Bank code 1ENY) as a search model. Molecular replacement solutions for the translation and rotation function were obtained from Crystallography and NMR software (CNS) (25). The CNS software package was utilized for molecular replacement, rigid-body refinement, simulated annealing, minimization, and B-factor refinement. The nucleotide cofactor was easily identified in a symmetry-averaged difference Fourier ( $F_o - F_c$ ) electron density map, verifying the correctness of the molecular replacement solution. Non-crystallographic symmetry restraints were applied after rigid body refinement and initial simulated annealing. NAD $^{+}$ , triclosan, and water molecules were added during several cycles of minimization followed by B-factor refinement, resulting in an  $R_{\text{factor}}$  of 19% and an  $R_{\text{free}}$  of 28% for the InhA-Genz-10850 complex, and an  $R_{\text{factor}}$  of 22.5% and an  $R_{\text{free}}$  of 28% for the InhA-triclosan complex. Non-crystallographic restraints were removed when significant differences were observed between the individual subunits present in the asymmetric unit. Inspection of  $F_o - F_c$  electron density maps calculated from an InhA:NADH model revealed significant additional density in the active sites of some of the subunits in the asymmetric unit. For the InhA-Genz-10850 complex, four of the six subunits contained product analog, whereas the remaining subunits lacked bound inhibitor. For the InhA-triclosan complex, two molecules of triclosan were clearly identified and placed in one subunit of the enzyme, whereas the other subunit contained only one molecule of triclosan. The differences may be related to negative cooperativity (23), which may translate into differences in inhibitor occupancy. Data collection statistics are presented in Table I.

**High Throughput Screening, Synthesis of Inhibitors, and  $K_i$  Measurements**—The high throughput screen measured the NADH-dependent catalysis of an octenoyl (C8:1  $\Delta$ 2)-CoA substrate as a decrease in 340 nm absorbance resulting from conversion of NADH to NAD $^{+}$ . This screen was run using samples synthesized as mixtures of up to 100 compounds. For the mixture containing Genz-10850, indole-5 carboxylic acid was reacted with 86 different amines in equimolar and limiting concentration. This mixture showed 40% inhibition when tested at a total concentration of 40  $\mu\text{M}$ . The 86 compounds in this mixture were then individually synthesized and tested. The most potent analogs from this mixture were amides of indole-5-carboxylic acid and 4-aryl-substi-

TABLE I  
Data collection and refinement statistics

Data collection	InhA:Genz-10850	InhA:Triclosan
Maximum resolution (Å)	2.7	2.6
Space group	C2	I2 <sub>1</sub> 2 <sub>1</sub> 2 <sub>1</sub>
a (Å)	101.0	94.8
b (Å)	83.3	103.9
c (Å)	193.1	189.6
α (°)	90	90
β (°)	95.2	90
γ (°)	90	90
Unique reflections	38,313	27,704
R <sub>sym</sub> (%) <sup>a</sup>	8.5	8.0
Completeness (%)	85.2	95.1
Redundancy	2.9	4.5
I/σ	13.2	10.3
Refinement statistics		
Resolution range (Å)	30-2.7	30-2.6
No. reflections	38,313	27,704
No. atoms/subunit		
Protein	11,964	11,964
NAD <sup>+</sup>	44	44
Ligand(s)	30	17/34
R <sub>cryst</sub> (%) <sup>b</sup>	19.0	22.5
R <sub>free</sub> (%) <sup>c</sup>	28.8	28.2
Average B-factors (Å <sup>2</sup> )		
Protein	31.6	26.5
NAD <sup>+</sup> /NADH	44.1	45.8
Inhibitors	47.7	38/52

<sup>a</sup>  $R_{sym} = \sum_h \sum_i |I_{hi} - \langle I_h \rangle| / \sum_h \sum_i I_{hi}$  where  $I_{hi}$  is the intensity of observation  $I$  of reflection  $h$ .

<sup>b</sup>  $R_{cryst} = \sum_h |F_{obs} - |F_{calc}|| / \sum_h |F_{obs}|$  where  $F_{obs}$  and  $F_{calc}$  are observed and calculated structure factors, respectively.

<sup>c</sup>  $R_{free}$  was calculated on 10% of the data omitted at random.

tuted piperazines. Subsequent synthesis of an array of piperazine analogs resulted in Genz-10850, which showed potent inhibition of InhA with an IC<sub>50</sub> value of 0.15 μM (Table II). In the case of Genz-8575 (Table III), a mixture of 13 malondialdehydes was reacted with an excess of (4-trifluoromethyl-pyrimidin-2-yl)-hydrazine. The resulting mixture had an inhibition of 38% against InhA at 40 μM. Deconvolution of this mixture yielded several active pyrazoles, the best of which (Genz-5542, 2-[3-(4-chloro-2-nitrophenyl)-pyrazol-1-yl]-4-trifluoromethyl-pyrimidine) showed 82% inhibition at 40 μM. Several analogs of this compound were prepared, among them Genz-8575, the result of replacing the chlorine atom with a nitro group. Genz-8575 displayed 91% inhibition at 40 μM against InhA (Table III). Substrate and co-enzyme concentrations in these screens were 250 and 100 μM, respectively. IC<sub>50</sub> values were determined by measuring the initial velocity over a broad range of inhibitor concentrations, plotting the fractional activity as a function of the log of the inhibitor concentration, and curve-fitting with a sigmoidal function.

Inhibition constants were determined under conditions of saturating substrate (200 μM substrate and 600 μM NADH) and variable inhibitor concentrations.  $K_i$  values were determined from the  $x$  intercept of a Dixon plot, assuming uncompetitive inhibition. For triclosan binding of InhA, we found a  $K_i$  of 8.5 μM, which differs from an earlier measurement of 0.22 μM (26). These discrepant results may in part be due to differences in the assay conditions, including the use of different chain length acyl-CoA substrates (C12:1 CoA versus C8:1 CoA).

**Minimal Inhibitory Concentration Determination**—Serial 10-fold dilutions of each *M. tuberculosis* culture were prepared in 7H9 medium (Difco) containing 0.05% glycerol, 0.02% Tween 80, and 10% oleate-albumin dextrose complex/saline. Each dilution was then plated on Middlebrook 7H10 medium containing 0.05% glycerol, and 10% oleate-albumin dextrose. Test compounds were added across a range of concentrations. The MIC<sub>99</sub> value was defined as the lowest concentration of the test compound that resulted in <1% growth as compared with drug-free controls.

**Mycobacterial Growth Inhibition Experiments**—*Klebsiella pneumoniae* (ATCC-12658), *Pseudomonas aeruginosa* (ATCC-27853), *Streptococcus pneumoniae* (ATCC-33400), *Staphylococcus aureus* (ATCC-29213), *Candida albicans* (ATCC-10231), and *Aspergillus niger* (ATCC-16404) were obtained from the ATCC. To determine bacterial growth inhibition, fresh cultures were grown at 37 °C in TB broth to an optical density of 0.2 at 550 nm. By using 96-well plates, 100 μl of this culture was added to 100 μl of TB broth containing compounds dissolved in 2 μl of Me<sub>2</sub>SO. When the optical density of the control wells reached 0.9, the

TABLE II  
Genz-10850 structure-activity relationship data

Genz-# <sup>a</sup>	R-group	IC <sub>50</sub> (μM)
10850	H	0.16
11918	1-CO <sub>2</sub> CH <sub>3</sub>	0.34
12637	2-Cl, 3-NHAc	>10
12638	2,7-I <sub>2</sub>	0.13
12639	2-NHAc	0.28
12640	2-NME <sub>2</sub>	0.91
12641	2-NHCHO	0.18
12643	2,4,7-Cl <sub>3</sub>	0.17
12644	2-NO <sub>2</sub>	0.13
12645	3-NO <sub>2</sub>	0.13
12646	2,7-Br <sub>2</sub>	0.12
13100	2-NHCOB	0.59
13108	2-NHCOCH <sub>2</sub> CH <sub>2</sub> CH <sub>3</sub>	0.46
13347	2-NEt <sub>2</sub>	>10
13348	2-OCH <sub>3</sub>	0.52
13349	4-OCH <sub>3</sub>	0.82

<sup>a</sup> These compounds were synthesized and assayed for their ability to inhibit InhA-mediated, NADH-dependent catalysis of an octenoyl-CoA substrate (see "Experimental Procedures"). IC<sub>50</sub> values refer to the concentration resulting in 50% inhibition of enzyme activity and were the lowest for Genz-10850.

TABLE III  
Genz-8575 structure-activity relationship data

Genz-#	R <sub>1</sub> -group	% Inhibition <sup>a</sup>	Genz-#	R <sub>2</sub> -group	% Inhibition <sup>a</sup>
5537		17	5542		86
5538		14	5984		10
5539		8	5985		17
5540		10	5986		9
5542		82	6341		60
7466		11	6356		54
8575		91	6371		27
			6386		5

<sup>a</sup> The right columns show the percent inhibition of InhA activity in the presence of 40 μM of each of these compounds. The best of this initial set of pyrazoles, Genz-5542, was further derived to generate analogs, including Genz-8575, which substituted a chlorine atom with a nitro group and that gave the best inhibition of all compounds in this series.

optical density of experimental wells was determined and used to derive percent inhibition of growth.

**Plasmodial Growth Inhibition Assays**—*P. falciparum* asexual blood-stage parasites were assayed *in vitro* in RPMI 1640-based culture medium containing 2.5 mg/ml hypoxanthine and 0.5% albumax (Invitrogen). Parasite cultures were then exposed to serial drug dilutions

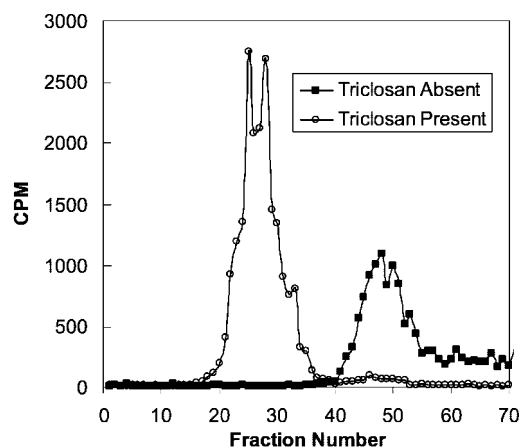


FIG. 1. **Triclosan-induced binding of [ $^{14}\text{C}$ ]NAD $^{+}$  to InhA.** The ability of InhA to bind [ $^{14}\text{C}$ ]NAD $^{+}$  in the presence of triclosan was determined by gel filtration chromatography as described under "Experimental Procedures." In the presence of triclosan, [ $^{14}\text{C}$ ]NAD $^{+}$  eluted with InhA proteins in the excluded volume of the Sephadex G-25 column (fractions 20–35). Without triclosan, free [ $^{14}\text{C}$ ]NAD $^{+}$  was eluted in the included volume (fractions 40–70).

over a 72 h period, with addition of tritiated hypoxanthine (7.5  $\mu\text{Ci}/\text{ml}$ ) after 48 h (27). After accounting for background counts/min with uninfected red blood cell controls, the percentage reduction in tritiated hypoxanthine equaled  $100 \times (\text{mean cpm of samples without drug} - \text{mean cpm of drug dilution samples}) / (\text{mean cpm of samples without drug})$ . This measurement represents a standard surrogate marker of growth inhibition. The  $\text{IC}_{50}$  and  $\text{IC}_{90}$  values were calculated by curve fitting and regression analyses.

#### RESULTS AND DISCUSSION

**Characteristics of Triclosan Binding to InhA**—To investigate the mode of triclosan binding to InhA, we purified and expressed this enzyme, performed initial velocity experiments, and measured the inhibition constants for triclosan. These experiments showed that triclosan binding was reversible and promoted by NAD $^{+}$  binding, suggesting that triclosan was uncompetitive with respect to NAD $^{+}$  and competed with the fatty acyl substrate.

Previous studies with *Escherichia coli* FabI have used gel filtration experiments to investigate whether triclosan is a slow binding inhibitor (22). To test whether the same holds true for triclosan inhibition of InhA, we performed similar experiments, testing [ $^{14}\text{C}$ ]NAD $^{+}$ , InhA, and triclosan in co-elution assays (Fig. 1). These showed that [ $^{14}\text{C}$ ]NAD $^{+}$  co-eluted with InhA only in the presence of triclosan. In the absence of triclosan, [ $^{14}\text{C}$ ]NAD $^{+}$  eluted in the included volume. These results demonstrate that the ternary inhibitory complex is in fact triclosan, NAD $^{+}$ , and InhA, consistent with our previously published  $K_m$  data that compared NAD $^{+}$  with NADH (28). These data indicate that triclosan is a slow binding inhibitor of InhA, by nature of its requirement to form a complex with NAD $^{+}$  in order to bind to the active site. These findings are consistent with earlier reports (9) of similar  $K_i$  values of triclosan inhibition of InhA and *E. coli* FabI, which were in the low micromolar range.

*In vitro* whole-cell assays demonstrated good activity of triclosan against INH-resistant and -sensitive *M. tuberculosis* strains (Table IV). Consistent with triclosan acting without the requirement for KatG-mediated activation, this compound was as effective against a strain carrying the KatG mutation S315T (conferring high-level INH resistance) as it was against wild-type strains. When tested against a low level, INH-resistant line containing an *inhA* promoter mutation leading to enzyme overexpression, triclosan activity was partially compromised at 35  $\mu\text{M}$ ; however, this compound remained fully active at 70  $\mu\text{M}$ . These data indicated that triclosan acts against InhA, as has now been confirmed by structural analysis (see below).

TABLE IV  
Triclosan is active against isoniazid-susceptible and -resistant *M. tuberculosis*

Strain	Mutation	Isoniazid MIC <sup>a</sup>	Triclosan MIC
M305	Wild type	1.5	20
M306	Wild type	1.5	25
M290	<i>inhA</i> promoter	7.5	60
M307 <sup>b</sup>	<i>katG</i> S315T	200	20

<sup>a</sup> MIC, minimal inhibitory concentration, expressed in  $\mu\text{M}$ .

<sup>b</sup> This strain is resistant to isoniazid, rifampicin, pyrazinamide, ethambutol, streptomycin, and kanamycin.

**Development of Chemically Tractable Inhibitors**—To identify additional lead compounds that act directly on *M. tuberculosis* InhA without the requirement for activation, we performed a high-throughput screen of ~500,000 compounds from a combinatorial library, using purified InhA as a target. This screen resulted in the identification of Genz-8575 and Genz-10850, which represent two new classes of InhA inhibitors (Table II and Table III; Fig. 2). In testing a series of about 300 Genz-10850 analogs, a structure-activity relation emerged whereby substitution was not allowed at carbon positions 2 or 3 of the piperazine ring (suggesting a steric clash with this part of the molecule) and where polar substitutions were allowed at the 2-position of the fluorenyl group (suggesting that this site is exposed to solvent). Alkylation or acylation of the indole nitrogen was not tolerated, in agreement with the role of this moiety as a hydrogen-bonding group. For the Genz-8575 analogs, a stringent requirement was detected at the trifluoromethylpyrimidine substituent, with more latitude available at the dinitrophenyl site. When tested against purified InhA, Genz-8575 and Genz-10850 displayed  $\text{IC}_{50}$  values of 2.4 and 0.16  $\mu\text{M}$ , respectively.

Although these inhibitors were selected from screens against *M. tuberculosis* InhA, the structural similarity between InhA and PfENR stimulated us to test them against the malarial enzyme. This revealed the  $\text{IC}_{50}$  for PfENR to be 32  $\mu\text{M}$  for Genz-8575, 18  $\mu\text{M}$  for Genz-10850, and 0.5  $\mu\text{M}$  for triclosan. The markedly disparate  $\text{IC}_{50}$  values between the ENRs could be due to the nature of the substrate-binding loop. The InhA loop is hydrophobic and contains an additional 10 residues when compared with the *E. coli* enzyme (FabI, see below), whereas the PfENR loop is a low complexity 45-amino acid insertion that is almost entirely polar.

**Crystal Structure of InhA with Triclosan**—Triclosan has been found to bind noncovalently to *E. coli* FabI (29–32), PfENR (21), and *Brassica napus* ENR (33). Here we determined the structure of InhA with triclosan to a 2.6-Å resolution. This revealed binding of the inhibitor in a similar site and orientation within the *M. tuberculosis* enzyme. Triclosan binding was found to overlap with the acyl substrate-binding pocket and was quite separate from the site of INH binding. In the crystal structure of the INH-NADH adduct (34) bound to InhA, the NADH part of the adduct was maintained in the NADH-binding site, and the INH portion of the adduct was projected into a pore formed by the rotation of the side chain of Phe<sup>149</sup>. Phe<sup>149</sup> was adjacent to the nicotinamide of NAD $^{+}$  in the substrate-bound form (35) and was rotated ~90° to optimize stacking with the pyridine ring of the isonicotinic acyl group. In contrast, in the InhA-triclosan complex, the hydroxyl-substituted ring of triclosan (the "A" ring) stacked with the nicotinamide ring of NAD $^{+}$  and formed a conserved hydrogen-bonding pattern with the 2'-hydroxyl group of NAD $^{+}$  and with Tyr<sup>158</sup> in the catalytic active site (21, 29–33). Hydrophobic contacts were responsible for the remaining interactions. The dichlorophenyl ring (the "B" ring) of triclosan was oriented orthogonally to the A ring, and the chlorines were projected toward the solvent.

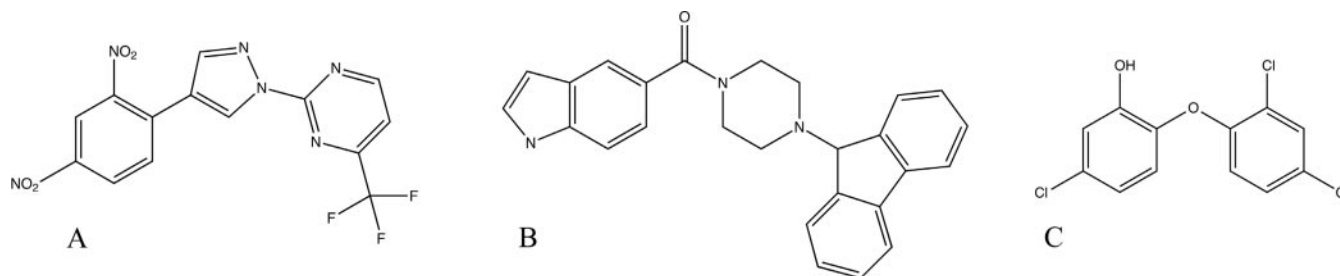


FIG. 2. Stick models of new enoyl ACP reductase inhibitors discovered from a high throughput combinatorial screen of recombinant *M. tuberculosis* InhA, illustrated alongside triclosan. A, Genz-8575; B, Genz-10850; and C, triclosan.

This mode of triclosan binding was conserved for the ENRs and for InhA (Fig. 3).

The second InhA:triclosan complex in the asymmetric unit showed binding of two triclosan molecules to the active site (Fig. 4). This has not been observed for any of the triclosan-ENR complexes solved to date. In the doubly-bound subunit, the mode of binding of one molecule of triclosan (designated TCN1) was identical to ENR:triclosan structures reported previously (21, 29–33) and was also identical to the binding we observed in the singly-bound *M. tuberculosis* InhA. The second molecule, designated TCN2, resided in an inverted orientation relative to TCN1 in an almost entirely hydrophobic area within the binding cavity. Both TCN1 and TCN2 were in identical low energy conformations and exhibited mostly van der Waals interactions between themselves and the protein. The binding of TCN2 to InhA was primarily mediated by van der Waals interactions with the hydrophobic side chains of residues Met<sup>103</sup>, Gly<sup>104</sup>, Phe<sup>149</sup>, Ala<sup>157</sup>, Met<sup>199</sup>, Ile<sup>202</sup>, Ile<sup>215</sup>, and Leu<sup>218</sup>. The majority of the interactions was from the substrate-binding loop that extended from residues 197 to 226 and that encompassed helices  $\alpha 6$  (residues 197–206) and  $\alpha 7$  (residues 209–226) (Fig. 4). The only polar residues within 4 Å were Gln<sup>100</sup> and Tyr<sup>158</sup>, which did not hydrogen-bond with TCN2. TCN2 stabilized the substrate-binding loop, resulting in an average B-factor of 54 Å<sup>2</sup>. This loop was only partially ordered (B-factor 70 Å<sup>2</sup>) in the subunit containing a single molecule of triclosan. Superposition of each subunit (singly- versus doubly-bound forms) revealed significant deviations in the C- $\alpha$  backbone in the substrate-binding loops that contacted triclosan (Fig. 5).

The presence of two molecules of triclosan in the active site of InhA could be attributed to the specificity of the *M. tuberculosis* enzyme for long to very long chain (C16 and greater) fatty acyl substrates. To accommodate long fatty acids, InhA possesses a hydrophobic substrate-binding loop (residues 197–226) that is ~10 residues longer (residues 203–212) than the corresponding loop in *E. coli* or *B. napus* FabI. The long loop in InhA, comprising one face of the active site, correlates with a substrate-binding cavity that is considerably larger in volume relative to ENRs from other organisms (acyl-binding site volume of 1,551 Å<sup>3</sup> for InhA, compared with 1,118 Å<sup>3</sup> for *E. coli* FabI and 1,257 Å<sup>3</sup> for *B. napus* ENR). These loop regions appear to be flexible, adjusting to the size of the substrate/inhibitor. Superimposition of the backbones of the doubly-bound inhibitor form of InhA:triclosan and InhA complexed with a fatty acyl substrate analog (C16-*N*-acetylcysteamine) produced a root mean square deviation of 0.6 Å. Further examination revealed that the C16-NAc and the two triclosan molecules showed strikingly similar modes of binding. The substrate-binding loops also superimposed well (Fig. 6). These data suggest that selective targeting of *M. tuberculosis* within the human host might be achieved using an inhibitor of the dual complex TCN1:TCN2.

**Structure of *M. tuberculosis* InhA Bound to Genz-10850**—The high throughput screen against InhA yielded compounds

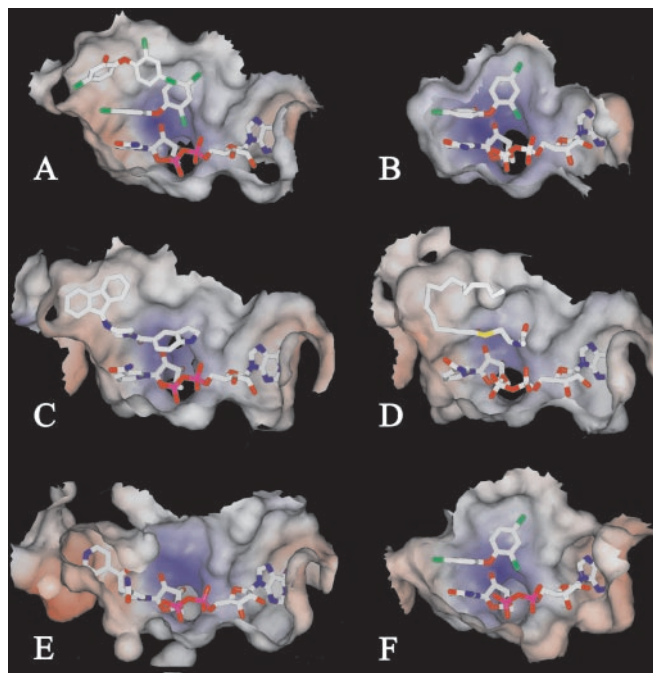


FIG. 3. Active sites of the *M. tuberculosis* and enoyl ACP reductases bound to inhibitors. A, cross-section through the surface of the InhA active site with bound triclosan, showing that InhA contains an additional triclosan-binding site compared with other ENRs. B, similar view of *E. coli* FabI with triclosan. C, cross-section through the Genz-10850-binding site in InhA, revealing the bulky fluorenyl group of this inhibitor that widens the fatty acid-binding loop. This is not observed in the NADH-bound structure that lacks an analogous bulky substituent. Note also the interaction of the nitrogen of the Genz-10850 indole ring with a NAD<sup>+</sup> phosphate oxygen. D, cross-section of the InhA active site with bound C16 fatty acyl substrate. Comparison with the inhibitor-bound forms of InhA shows that both substrate and inhibitor utilize the 2'-OH ribose of NADH as a hydrogen-bonding partner. E, cross-section of the InhA active site with bound INH. The activated form of INH covalently attaches to the nicotinamide ring of NADH. F, cross-section of the *B. napus* active site with bound triclosan.

that were chemically very different to triclosan, despite similar modes of inhibition. To gain insights into the molecular details of how this new group of compounds binds to InhA, we solved the x-ray crystal structure of the InhA:Genz-10850 complex. Electron density for a single molecule of Genz-10850 was observed in the InhA active site (Fig. 7), in the area normally occupied by triclosan or fatty-acyl substrate (Fig. 3, A and D). Comparison of this structure with a previous structure of InhA: C16-NAc (23, 34, 35) suggested that Genz-10850 also occupies a region of the active site that is normally bound by substrate/product. This interpretation was supported by kinetic studies of members of the two classes of Genzyme compounds, showing that they were competitive with the enoyl-CoA substrate (data not shown). The Genz-10850 carbonyl group formed a hydrogen-bonding network with the 2'-ribose hydroxyl of the NAD<sup>+</sup>

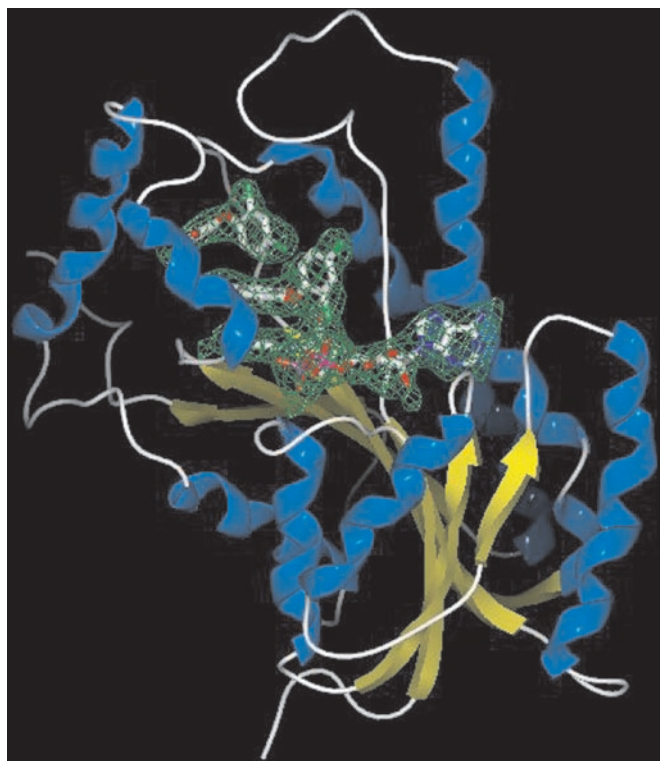


FIG. 4. Structure of the InhA-triclosan complex with an  $F_o - F_c$  map contoured at  $3\sigma$ . Triclosan was omitted from the electron density calculations to prevent bias. Helices are depicted in blue, and the  $\beta$ -strands are represented in yellow. The two molecules of triclosan occupied the substrate-binding portion of the active site. The hydroxyl groups of the A rings were oriented in opposite directions, whereas the dichlorophenyl rings (B rings) did not stack.

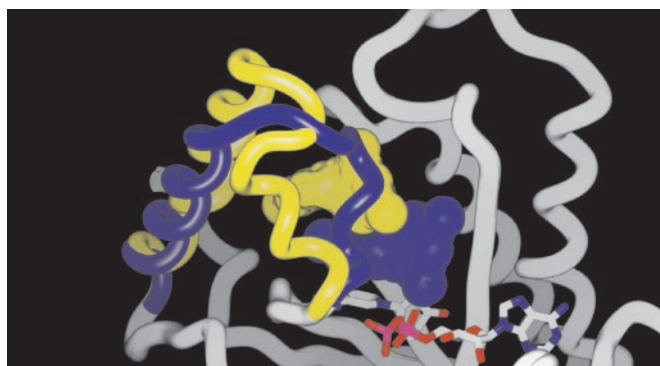


FIG. 5. Superposition of the two subunits of InhA present in the asymmetric unit of the InhA-triclosan complex. Superimposed worm diagrams representing the backbone of each subunit. The  $NAD^+$  cofactor is depicted in stick form, and triclosan is shown as a molecular surface (TCN1 in dark blue and TCN2 in dark yellow). White represents regions of InhA without significant backbone deviations. Colored worms represent the conformation of the substrate-binding loop ( $\alpha 6$  and  $\alpha 7$ ) in the singly- (light blue) and doubly- (light yellow)-bound forms of InhA. The presence of TCN2 results in a pronounced shift of the loop in order to accommodate the two triclosan molecules.

and the side chain of the catalytic residue Tyr<sup>158</sup>. Binding of the bulky fluorenyl group occurred within the substrate-binding pocket that normally sees the long acyl chain of the substrate. Genz-10850 binding resulted in a wider fatty acyl substrate-binding groove (compared with the  $NAD^+$  bound structure) as well as additional van der Waals interactions with the hydrophobic residues Gly<sup>96</sup>, Met<sup>103</sup>, Phe<sup>149</sup>, Met<sup>155</sup>, Pro<sup>156</sup>, Ala<sup>157</sup>, Met<sup>161</sup>, Pro<sup>193</sup>, Ala<sup>198</sup>, Ile<sup>215</sup>, and Leu<sup>218</sup>. This information was in agreement with the observed structure-activity relationship for Genz-10850, which indicated that sub-

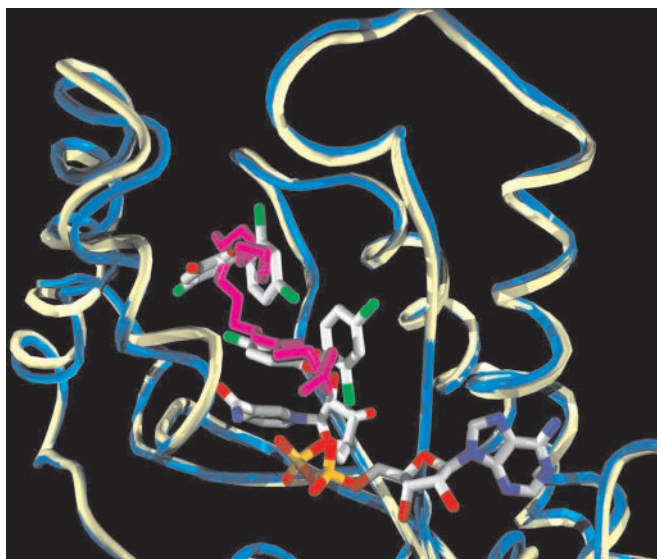


FIG. 6. Superposition of the InhA-C16-Nac and InhA-triclosan complexes. White worms represent the C- $\alpha$  trace of InhA:C16-Nac, and blue worms represent the C- $\alpha$  trace of the InhA:triclosan structure. The C16-Nac and the two molecules of triclosan exhibit remarkably similar modes of binding.

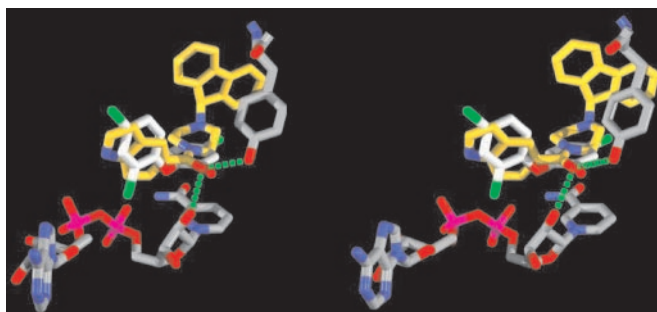


FIG. 7. Stereo view overlay of Genz-10850 and triclosan reveals that both inhibitors maintain similar hydrogen-bonding interactions with  $NAD^+$  and the catalytic residue Tyr<sup>158</sup>.

stitutions on the piperazine ring would sterically clash with Phe<sup>149</sup>, whereas polar substitutions at the 2-position of the fluorene moiety would be tolerated due to its exposure to solvent. Alkylation or acylation of the indole nitrogen would disrupt a weak hydrogen bond between Genz-10850 and a  $NAD^+$  phosphate oxygen.

*Comparison of InhA:Genz-10850, InhA:Triclosan, and Other ENR Inhibitors*—Superimposition of the backbones of the two InhA-inhibitor complexes revealed that the A and B ring of triclosan overlaid the piperazine and indole groups of Genz-10850, respectively. The triclosan hydroxyl group and the Genz-10850 carbonyl group occupied similar positions and retained a similar hydrogen-bonding network with the 2'-ribose hydroxyl of the dinucleotide cofactor and the Tyr<sup>158</sup> side chain. Van der Waals interactions accounted for the remainder of the interactions between Genz-10850 and protein, and the fluorenyl moiety ordered the substrate-binding loop. Our structural model of the mechanism of action for these inhibitors is consistent with the structure-activity relationships identified in other organisms (21, 29–33). Several reports described the mode of binding of triclosan to the ENRs from *E. coli* (29–32), *B. napus* (33), and *P. falciparum* (21). All maintained the hydrogen-bonding network between the A ring, a catalytic tyrosine,  $NAD^+$  cofactor, and a catalytic lysine. The stacking interactions between the A ring and  $NAD^+$  were also conserved.

TABLE V  
Genz-8575 is active against multidrug resistant *M. tuberculosis*

*M. tuberculosis* isolates were cultured from clinical patient samples. The presence of point mutations in selected regions of *katG*, *InhA*, *ahpC*-oxyR, and *kasA* was assessed using molecular beacon probes as described previously (42). Mutations were detected only in *KatG* and *InhA* (shown below).

Strain	Antibiogram <sup>a</sup>	<i>katG</i> allele <sup>b</sup>	<i>InhA</i> allele	Isoniazid MIC <sup>b</sup>	Genz-8575 MIC <sup>c</sup>
H37Rv	Pan-susceptible	WT	WT	1.5	2.5
TN913	Pan-susceptible	WT	WT	1.5	1.25
TN7791	I	S315N	WT	ND	1.25
TN5038	I, R	L634F	WT	300	1.25
TN6117	I, R, Z	IS6110 insertion	WT	>300	15
TN565	I, R, S, E, Z, H, K, C	S315T	WT	>300	30
TN5369	I, Z	WT	A239T	>300	25
TN6134	I, R, S	WT	I194T	75	7.5

<sup>a</sup> C, ciprofloxacin; E, ethambutol; H, ethionamide; I, INH; K, kanamycin; R, rifampicin; S, streptomycin; Z, pyrazinamide. Fingerprint analysis using the ubiquitous insertion element *IS6110* indicated distinct genetic backgrounds for each strain.

<sup>b</sup> WT, wild-type; ND, not determined.

<sup>c</sup> MIC (minimum inhibitory concentrations) are expressed in  $\mu\text{M}$ .

In addition to triclosan analogs (9, 21), other ENR inhibitors have been described, including derivatives of diazaborines (8), imidazoles (36), indoles (37), and aminopyridines (38). Perozzo *et al.* (21) reported a series of triclosan derivatives utilized in inhibitor studies with PfENR. Common features associated with the more potent derivatives included a hydroxyphenyl ring bridged with either a dichlorophenyl or a naphthol ring. Substitution of the hydroxyl group of the A ring was not tolerated, whereas the bridging atom could be either an oxygen or a nitrogen but not a sulfur or a carbon (9, 39). Variability was allowed in the remainder of the molecule, which tended to be highly hydrophobic. Binding of thienodiazaborine and benzo-diazaborine to *E. coli* FabI has also been described (40). This report showed that the diazaborines covalently modified  $\text{NAD}^+$ , whereas the bicyclic rings formed face-to-face stacking interactions with the nicotinamide ring and hydrogen-bonded to Tyr<sup>156</sup>. Heerding *et al.* (36) reported the crystal structure of *E. coli* FabI complexed to an inhibitor derived from disubstituted-imidazoles (Protein Data Bank entry 1I2Z). In their analysis, the inhibitor stacked with the nicotinamide ring of  $\text{NAD}^+$ , whereas the unsubstituted nitrogen of the imidazole interacted with the catalytic tyrosine. The crystal structure of *E. coli* FabI bound to an indole-derived inhibitor has also been described (37) and showed that the 4-hydroxybenzamide moiety hydrogen-bonded to the catalytic Tyr<sup>156</sup> of FabI and had orthogonal  $\pi$ -stacking interactions with Tyr<sup>146</sup> (Protein Data Bank entry 1I30). Similar results were reported by Miller *et al.* (38), who reported the structure of *E. coli* FabI bound to two aminopyridine-based inhibitors. These inhibitors stacked with  $\text{NAD}^+$  and formed hydrogen bonds to a conserved catalytic tyrosine Tyr<sup>156</sup> (the equivalent of Tyr<sup>158</sup> in *InhA*), as well as additional hydrogen bond interactions with either phosphates on  $\text{NAD}^+$  or two hydrogen bonds to the Ala<sup>95</sup> backbone. We note that lead optimization studies have been initiated on aminopyridine-based inhibitor hits (41), identified through previous high-throughput screens against *S. aureus* FabI (38). Iterative medicinal chemistry and structure-based drug design improved the inhibitory potency of the original lead compound by >350-fold, and the final compound retained the moieties implicated as important for stacking and hydrogen-bonding. In the structure of *InhA* with bound  $\text{NAD}^+$  and the product analog C16-Nac, a similar hydrogen-bonding pattern was observed for the carbonyl oxygen of the C16-Nac. The remainder of the product analog interacted with the substrate-binding loop, restoring order to this loop upon binding. These studies, in concert with our crystal structures of *InhA*:triclosan and *InhA*:Genz-10850, accentuate the importance of the hydrogen bonding network, stacking interactions with either  $\text{NAD}^+$  or catalytic residues, and the presence of a hydrophobic moiety to mimic a fatty acyl substrate.

TABLE VI  
Genz-8575 showed no significant influence on the inhibition of growth of six common infectious agents when compared to *M. tuberculosis* and *P. falciparum*

Species	Percent Inhibition <sup>a</sup>	Triclosan MIC
	%	$\mu\text{M}$
<i>Kl. pneumoniae</i> <sup>b</sup>	0	50
<i>P. aeruginosa</i> <sup>b</sup>	2	50
<i>S. pneumoniae</i> <sup>c</sup>	2	50
<i>S. aureus</i> <sup>c</sup>	20	50
<i>C. albicans</i>	1	25
<i>A. niger</i>	56	25

<sup>a</sup> Percent inhibition of growth relative to untreated culture.

<sup>b</sup> Gram-negative.

<sup>c</sup> Gram-positive.

*Activity of ENR Inhibitors against M. tuberculosis*—Although Genz-8575 showed less activity *in vitro* against purified recombinant *InhA*, this compound showed good activity in whole-cell assays against several drug-susceptible and drug-resistant strains of *M. tuberculosis*, with MIC values in the range of 1.25 to 30  $\mu\text{M}$  (Table V). When compared with Pan-susceptible strains (H37Rv and TN913), the strains containing mutations in the *katG* gene (T7791, TN5038, TN6117, and TN565) displayed a >200-fold increase in MIC values required for INH inhibition. This agrees with earlier evidence concluding that INH is a prodrug that must be activated by *KatG* (16). In contrast, Genz-8575 retained equal activity against the TN5038 strain and weaker activity against the TN6117 and TN565 multidrug resistant strains of *M. tuberculosis*. This suggests a mode of action independent of *KatG* activation, circumventing the most prominent method of acquiring drug resistance in this pathogen. The strains TN5369 and TN6134, containing point mutations in the *inhA* allele, displayed decreased sensitivity to INH (Table V).

We undertook modeling studies to ascertain the structural basis of resistance conferred by these mutations. The I194T of strain TN6134 mapped to a region of the active site bordering the nucleotide cofactor. Mutation of a residue from polar to hydrophobic resulted in unfavorable interactions between residue 194 and the nicotinamide ring of  $\text{NAD}^+$ . As inhibitors depend not only on interactions with the target protein, but also with the cofactor, this effectively decreases the affinity of the inhibitors for the enzyme. For the A239T mutations, the interpretation is less evident. Ala<sup>239</sup> is buried by several hydrophobic residues including Ile<sup>21</sup>, Ile<sup>25</sup>, Val<sup>28</sup>, Ala<sup>235</sup>, Val<sup>238</sup>, Val<sup>242</sup>, and Cys<sup>243</sup>. Replacing the hydrophobic Ala<sup>239</sup> with a threonine could serve to destabilize this hydrophobic cluster, leading to longer range effects that ultimately perturb the  $\text{NADH}$ -binding pocket. Because many of these inhibitors rely on  $\text{NADH}$  for stacking and hydrogen-bonding interactions, a

TABLE VII  
*InhA* inhibitors are active against drug-resistant *P. falciparum*

Line	Resistant to <sup>a, b</sup>	Genz-10850 <sup>c</sup>		Genz-8575		Triclosan	
		IC <sub>50</sub>	IC <sub>90</sub>	IC <sub>50</sub>	IC <sub>90</sub>	IC <sub>50</sub>	IC <sub>90</sub>
FCB	CQ, QN, CYC	21.1 ± 1.7	38.1 ± 0.9	11.2 ± 0.6	21.8 ± 0.3	0.4 ± 0.1	5.2 ± 0.1
106/1	QN, CYC	31.5 ± 1.6	56.7 ± 1.3	16.3 ± 0.5	22.6 ± 0.3	0.9 ± 0.3	4.1 ± 0.2
Dd2	CQ, QN, PYR, SDX	21.6 ± 0.1	42.3 ± 0.2	ND	ND	0.4 ± 0.2	4.3 ± 0.2
HB3	PYR	14.4 ± 0.4	24.0 ± 0.2	10.4 ± 0.3	21.4 ± 0.3	0.2 ± 0.1	4.9 ± 0.4
3D7	SDX	16.9 ± 1.3	24.2 ± 0.1	11.1 ± 0.3	22.2 ± 0.2	0.7 ± 0.1	2.8 ± 0.1

<sup>a</sup> CQ, chloroquine; QN, quinine; CYC, cycloguanil; PYR, pyrimethamine; SDX, sulfadoxine; ND, not determined.

<sup>b</sup> Phenotypes were compiled from recent literature (43-46) and unpublished data. The Dd2 and 3D7 sulfadoxine phenotypes were ascertained in zero folate conditions and were reported to be high and low level resistance, respectively (46).

<sup>c</sup> Inhibition values are in  $\mu\text{M}$  and are reported as means  $\pm$  S.E. calculated from [<sup>3</sup>H]hypoxanthine incorporation assays performed on two three separate occasions in duplicate.

disturbance in the NADH-binding site would be reflected by the observed 10–20-fold increase in the Genz-8575 IC<sub>50</sub> values. For Genz-10850, the reduced whole-cell potency against these strains (IC<sub>50</sub> >30  $\mu\text{M}$ , data not shown), contrasting with the sub-micromolar affinity of this inhibitor for the purified enzyme, may result from poor uptake across the mycobacterial cell wall and perhaps solubility issues.

**Broad Spectrum Efficacy of Genz-8575**—To test the efficacy and toxicity of Genz-8575 against a range of pathogenic bacteria and yeast, we performed growth inhibition experiments with Gram-positive and Gram-negative organisms (Table VI). Genz-8575 showed no significant influence on the inhibition of growth of six common infectious agents, in contrast to its activity against *M. tuberculosis* and *P. falciparum*. In a separate assay, Genz-10850 was found to inhibit growth of *S. pneumoniae* with an IC<sub>50</sub> greater than 9.2  $\mu\text{M}$ . Preliminary acute intraperitoneal toxicity studies in mice showed that Genz-8575 and Genz-10850 were both well tolerated at doses up to 200 mg/kg.

**Activity of ENR Inhibitors against *P. falciparum***—The Genz-10850 and Genz-8575 compounds, identified using a *M. tuberculosis* *InhA* screen, displayed surprisingly good inhibition of *P. falciparum* growth at low micromolar concentrations (IC<sub>50</sub> ranges of 14 to 32  $\mu\text{M}$  and 10 to 16  $\mu\text{M}$ , respectively), with these compounds displaying equal efficacy against drug-resistant and -sensitive *P. falciparum* strains (Table VII). The best potency was nevertheless observed with triclosan, which gave IC<sub>50</sub> values of 0.2–0.9  $\mu\text{M}$  against drug-sensitive, single drug-resistant, and multidrug-resistant strains of *P. falciparum* (Table VII). This potent activity is comparable with *E. coli* (14). Analysis of [<sup>14</sup>C]acetate-labeled fatty acid synthesis in triclosan-treated cultures of both *M. tuberculosis* and *P. falciparum* showed a marked decrease in the extent of incorporation of the radiolabeled precursor into long chain fatty acids (20) (data not shown). Interestingly, the Genz-8575, Genz-10850, and triclosan IC<sub>50</sub> values obtained *in vitro* with purified PfENR were 32, 18  $\mu\text{M}$ , and 0.5  $\mu\text{M}$ , respectively, very similar to the whole-cell assay results, suggesting good uptake of the product analog. This is in direct contrast to the analogous studies with *M. tuberculosis* *InhA*, where IC<sub>50</sub> values increased dramatically in the whole-cell studies, presumably because of the presence of the mycobacterial cell wall that can impact differently on uptake of the individual compounds.

Both tuberculosis and malaria primarily affect individuals in the developing world and can be caused by strains that have acquired resistance to all existing, inexpensive chemotherapeutic regimens. Thus, there is an urgent need to develop novel, effective, and affordable drugs to treat both diseases. The FAS-II enzymes, which mediate fatty acid biosynthesis, represent superb targets that are essential for pathogen growth and that are not found in humans. The FAS-II ENR is particularly attractive, as its inactivation in temperature-sensitive mutants has been shown to induce lysis in mycobacterial cells (15), and

the activity of this enzyme appears essential for the normal development of plasmodial parasites (19, 20). Our high throughput screening has identified two new chemical entities that are active against drug-resistant strains of both organisms. Very good activity against both organisms was also found using the ENR inhibitor triclosan. Based on our structural data and incorporating medicinal chemistry approaches, we are now channeling efforts to generate derivatives of these molecular scaffolds that improve on potency and the limited bioavailability seen with triclosan. The chemically tractable nature of these ENR inhibitors and their analysis by x-ray crystallography provide a foundation on which to aim to develop a new family of compounds for use against these devastating pathogens.

#### REFERENCES

- Bloch, K. (1977) *Adv. Enzymol. Relat. Areas Mol. Biol.* **45**, 1–84
- Waller, R. F., Keeling, P. J., Donald, R. G., Striepen, B., Handman, E., Lang-Unnasch, N., Cowman, A. F., Besra, G. S., Roos, D. S., and McFadden, G. I. (1998) *Proc. Natl. Acad. Sci. U. S. A.* **95**, 12352–12357
- Fichera, M. E., and Roos, D. S. (1997) *Nature* **390**, 407–409
- Kohler, S., Delwiche, C. F., Denny, P. W., Tilney, L. G., Webster, P., Wilson, R. J., Palmer, J. D., and Roos, D. S. (1997) *Science* **275**, 1485–1489
- Palmer, J. D., and Delwiche, C. F. (1996) *Proc. Natl. Acad. Sci. U. S. A.* **93**, 7432–7435
- McFadden, G. I., and Waller, R. F. (1997) *Bioessays* **19**, 1033–1040
- Jomaa, H., Wiesner, J., Sanderbrand, S., Altincicek, B., Weidemeyer, C., Hintz, M., Turbachova, I., Eberl, M., Zeidler, J., Lichtenthaler, H. K., Soldati, D., and Beck, E. (1999) *Science* **285**, 1573–1576
- Roujeinikova, A., Sedelnikova, S., de Boer, G. J., Stuitje, A. R., Slabas, A. R., Rafferty, J. B., and Rice, D. W. (1999) *J. Biol. Chem.* **274**, 30811–30817
- Heath, R. J., Yu, Y. T., Shapiro, M. A., Olson, E., and Rock, C. O. (1998) *J. Biol. Chem.* **273**, 30316–30320
- Hayashi, T., Yamamoto, O., Sasaki, H., Kawaguchi, A., and Okazaki, H. (1983) *Biochem. Biophys. Res. Commun.* **115**, 1108–1113
- Jackowski, S., Murphy, C. M., Cronan, J. E., Jr., and Rock, C. O. (1989) *J. Biol. Chem.* **264**, 7624–7629
- Nishida, I., Kawaguchi, A., and Yamada, M. (1986) *J. Biochem. (Tokyo)* **99**, 1447–1454
- Tsay, J. T., Rock, C. O., and Jackowski, S. (1992) *J. Bacteriol.* **174**, 508–513
- Banerjee, A., Dubnau, E., Quemard, A., Balasubramanian, V., Um, K. S., Wilson, T., Collins, D., de Lisle, G., and Jacobs, W. R., Jr. (1994) *Science* **263**, 227–230
- Vilcheze, C., Morbidoni, H. R., Weisbrod, T. R., Iwamoto, H., Kuo, M., Sacchettini, J. C., and Jacobs, W. R., Jr. (2000) *J. Bacteriol.* **182**, 4059–4067
- Zhang, Y., Heym, B., Allen, B., Young, D., and Cole, S. (1992) *Nature* **358**, 591–593
- Escalante, P., Ramaswamy, S., Sanabria, H., Soini, H., Pan, X., Valiente-Castillo, O., and Musser, J. M. (1998) *Tubercle Lung Dis.* **79**, 111–118
- Grassberger, M. A., Turnowsky, F., and Hildebrandt, J. (1984) *J. Med. Chem.* **27**, 947–953
- McLeod, R., Muench, S. P., Rafferty, J. B., Kyle, D. E., Mui, E. J., Kirisits, M. J., Mack, D. G., Roberts, C. W., Samuel, B. U., Lyons, R. E., Dorris, M., Milhous, W. K., and Rice, D. W. (2001) *Int. J. Parasitol.* **31**, 109–113
- Surolia, N., and Surolia, A. (2001) *Nat. Med.* **7**, 167–173
- Perozzo, R., Kuo, M., Sidhu, A. S., Valiyaveetil, J. T., Bittman, R., Jacobs, W. R., Jr., Fidock, D. A., and Sacchettini, J. C. (2002) *J. Biol. Chem.* **277**, 13106–13114
- Heath, R. J., Rubin, J. R., Holland, D. R., Zhang, E., Snow, M. E., and Rock, C. O. (1999) *J. Biol. Chem.* **274**, 11110–11114
- Dessen, A., Quemard, A., Blanchard, J. S., Jacobs, W. R., Jr., and Sacchettini, J. C. (1995) *Science* **267**, 1638–1641
- Otwinowski, Z., and Minor, W. (1997) *Methods Enzymol.* **276**, 307–326
- Brunger, A. T., Adams, P. D., Clore, G. M., DeLano, W. L., Gros, P., Grosse-Kunstleve, R. W., Jiang, J. S., Kuszewski, J., Nilges, M., Pannu, N. S., Read, R. J., Rice, L. M., Simonson, T., and Warren, G. L. (1998) *Acta Crystallogr. Sect. D Biol. Crystallogr.* **54**, 905–921
- Parikh, S. L., Xiao, G., and Tonge, P. J. (2000) *Biochemistry* **39**, 7645–7650

27. Fidock, D. A., Nomura, T., and Wellems, T. E. (1998) *Mol. Pharmacol.* **54**, 1140–1147
28. Quemard, A., Sacchettini, J. C., Dessen, A., Vilcheze, C., Bittman, R., Jacobs, W. R., Jr., and Blanchard, J. S. (1995) *Biochemistry* **34**, 8235–8241
29. Ward, W. H., Holdgate, G. A., Rowsell, S., McLean, E. G., Pauptit, R. A., Clayton, E., Nichols, W. W., Colls, J. G., Minshull, C. A., Jude, D. A., Mistry, A., Timms, D., Camble, R., Hales, N. J., Britton, C. J., and Taylor, I. W. (1999) *Biochemistry* **38**, 12514–12525
30. Qiu, X., Janson, C. A., Court, R. I., Smyth, M. G., Payne, D. J., and Abdel-Meguid, S. S. (1999) *Protein Sci.* **8**, 2529–2532
31. Stewart, M. J., Parikh, S., Xiao, G., Tonge, P. J., and Kisker, C. (1999) *J. Mol. Biol.* **290**, 859–865
32. Levy, C. W., Roujeinikova, A., Sedelnikova, S., Baker, P. J., Stuitje, A. R., Slabas, A. R., Rice, D. W., and Rafferty, J. B. (1999) *Nature* **398**, 383–384
33. Roujeinikova, A., Levy, C. W., Rowsell, S., Sedelnikova, S., Baker, P. J., Minshull, C. A., Mistry, A., Colls, J. G., Camble, R., Stuitje, A. R., Slabas, A. R., Rafferty, J. B., Pauptit, R. A., Viner, R., and Rice, D. W. (1999) *J. Mol. Biol.* **294**, 527–535
34. Rozwarski, D. A., Grant, G. A., Barton, D. H., Jacobs, W. R., Jr., and Sacchettini, J. C. (1998) *Science* **279**, 98–102
35. Rozwarski, D. A., Vilcheze, C., Sugantino, M., Bittman, R., and Sacchettini, J. C. (1999) *J. Biol. Chem.* **274**, 15582–15589
36. Heering, D. A., Chan, G., DeWolf, W. E., Fosberry, A. P., Janson, C. A., Jaworski, D. D., McManus, E., Miller, W. H., Moore, T. D., Payne, D. J., Qiu, X., Rittenhouse, S. F., Slater-Radosti, C., Smith, W., Takata, D. T., Vaidya, K. S., Yuan, C. C., and Huffman, W. F. (2001) *Bioorg. Med. Chem. Lett.* **11**, 2061–2065
37. Seefeld, M. A., Miller, W. H., Newlander, K. A., Burgess, W. J., Payne, D. J., Rittenhouse, S. F., Moore, T. D., DeWolf, W. E., Jr., Keller, P. M., Qiu, X., Janson, C. A., Vaidya, K., Fosberry, A. P., Smyth, M. G., Jaworski, D. D., Slater-Radosti, C., and Huffman, W. F. (2001) *Bioorg. Med. Chem. Lett.* **11**, 2241–2244
38. Miller, W. H., Seefeld, M. A., Newlander, K. A., Uzinskas, I. N., Burgess, W. J., Heering, D. A., Yuan, C. C., Head, M. S., Payne, D. J., Rittenhouse, S. F., Moore, T. D., Pearson, S. C., Berry, V., DeWolf, W. E., Jr., Keller, P. M., Polizzi, B. J., Qiu, X., Janson, C. A., and Huffman, W. F. (2002) *J. Med. Chem.* **45**, 3246–3256
39. Heath, R. J., Li, J., Roland, G. E., and Rock, C. O. (2000) *J. Biol. Chem.* **275**, 4654–4659
40. Baldock, C., Rafferty, J. B., Sedelnikova, S. E., Baker, P. J., Stuitje, A. R., Slabas, A. R., Hawkes, T. R., and Rice, D. W. (1996) *Science* **274**, 2107–2110
41. Payne, D. J., Miller, W. H., Berry, V., Brosky, J., Burgess, W. J., Chen, E., DeWolf, W. E., Jr., Fosberry, A. P., Greenwood, R., Head, M. S., Heering, D. A., Janson, C. A., Jaworski, D. D., Keller, P. M., Manley, P. J., Moore, T. D., Newlander, K. A., Pearson, S., Polizzi, B. J., Qiu, X., Rittenhouse, S. F., Slater-Radosti, C., Salyers, K. L., Seefeld, M. A., Smyth, M. G., Takata, D. T., Uzinskas, I. N., Vaidya, K., Wallis, N. G., Winram, S. B., Yuan, C. C., and Huffman, W. F. (2002) *Antimicrob. Agents Chemother.* **46**, 3118–3124
42. Rhee, J. T., Piatek, A. S., Small, P. M., Harris, L. M., Chaparro, S. V., Kramer, F. R., and Alland, D. (1999) *J. Clin. Microbiol.* **37**, 1764–1770
43. Peterson, D. S., Walliker, D., and Wellems, T. E. (1988) *Proc. Natl. Acad. Sci. U. S. A.* **85**, 9114–9118
44. Su, X., Kirkman, L. A., Fujioka, H., and Wellems, T. E. (1997) *Cell* **91**, 593–603
45. Cooper, R. A., Ferdig, M. T., Su, X. Z., Ursos, L. M., Mu, J., Nomura, T., Fujioka, H., Fidock, D. A., Roepe, P. D., and Wellems, T. E. (2002) *Mol. Pharmacol.* **61**, 35–42
46. Wang, P., Read, M., Sims, P. F., and Hyde, J. E. (1997) *Mol. Microbiol.* **23**, 979–986